VII International Conference on Computational Methods for Coupled Problems in Science and Engineering
COUPLED PROBLEMS 2017
M. Papadrakakis, E. Oñate and B. Schrefler (Eds)

THE COMPARISON OF DIFFERENT ACOUSTIC APPROACHES IN THE SIMULATION OF HUMAN PHONATION

Jan Valášek*, Manfred Kaltenbacher† and Petr Sváček††

*,†† Department of Technical Mathematics
Faculty of Mechanical Engineering, CTU in Prague
Karlovo nam. 13, 121 35 Praha 2, Czech Republic
e-mail: jan.valasek1@fs.cvut.cz, petr.svacek@fs.cvut.cz

†Institute for Mechanics and Mechatronics
Technical University Vienna
Getreidemarkt 9, 1060 Wien, Austria
e-mail: manfred.kaltenbacher@tuwien.ac.at - Web page: http://www.mec.tuwien.ac.at

Key words: Fluid-Structure Interaction, 2D Navier-Stokes equations, Linear Elasticity, Aeroacoustic Analogies, Perfectly Matched Layer

Abstract. This contribution deals with mathematical modelling and numerical simulation of the human phonation process. This phenomena is described as a coupled problem composed of the three mutually coupled physical fields: the deformation of elastic body, the fluid flow and the acoustics. For the sake of simplicity only a two-dimensional model problems is considered in this paper. The fluid-structure interaction problem is described by the incompressible Navier-Stokes equations, by the linear elasticity theory and by the interface conditions. In order to capture the motion of the fluid domain the arbitrary Lagrangian-Eulerian method is used. The strongly coupled partitioned scheme is used for solution of the coupled fluid-structure problem. For solution of acoustics the acoustic analogies are used. Two analogies are compared - the Lighthill analogy and convected perturbation wave equation. The influence of acoustic field back to fluid as well as to structure is neglected. The numerical approximation of all three physical domains is perforemd with the aid of the finite element method. The numerical results present sound propagation through the model of the vocal tract.

1 INTRODUCTION

The human phonation is very interesting phenomenon and a complex topic of ongoing research, see e.g. [7]. A better understanding of the human phonation process can help physicians and therapists to improve treatment of people with voice disorders, where the

economic losses due to voice malfunction just in USA is estimated up to $160 billion per year, [9]. Recently due to practical inaccessibility of human organs numerical simulations have become to be an important tool used in the research.

The human phonation is a multi-physical problem consisting of three coupled physical fields – the deformation of the vocal folds (elastic body), the fluid flow and the acoustics together with all relevant coupling terms. It is sometimes summarized under fluid-structure-acoustic interaction (FSAI) problem. The mutual coupling between the fluid and the structure is usually strong, i.e. each physical field influences the other one. On the other hand the acoustic field in the considered problem depends on both the fluid and structure fields, but the influence of the acoustic back to the flow field as well as to the elastic body motion can be neglected. Thus it is possible to use only the so-called forward coupling from the fluid flow to the acoustic field, see [11].

There are a lot of papers covering the subject of human phonation ranging from studies of purely flow simulation in 2D or 3D domains like [10] or reports with prescribed motion of vocal folds, see for example [8], up to even 3D simulation of aeroacoustic problem, see e.g. [11]. The critical part for acoustic simulation is reliable solution of fluid flow. In general the maximal velocity lies noticeably under 0.3 Mach number (stated as incompressible limit), the flow passing the glottis is characterized by quite complex turbulent structure. This results in high computation demand namely in 3D, see [10].

This contribution presents the 2D aeroacoustic computation based on fluid-structure interaction (FSI) simulations, where the comparison of results acquired by the Lighthill analogy and the perturbed convective wave equation (PCWE) is shown. Similar hybrid approach has been already adopted in e.g. [11]. Furthermore, to include the effects of time-dependent computational domain for the fluid flow the Arbitrary Lagrangian-Eulerian (ALE) method was used. The linear elasticity theory was used for description of the elastic structure motion. Finally, the acoustics was modelled by Lighthill acoustic analogy and PCWE, [4]. The perfectly matched layer (PML) technique with inverse mapping was applied to solve the open-domain problem, see [5].

The numerical model is based on the finite element method (FEM), which is used for all three physical domains. For stabilization of the fluid flow simulation, the modified Streamline-Upwind/Petrov-Galerkin stabilization is utilized, [3]. In the end the numerical results of flow induced vibration and sound propagation through vocal tract are presented. The pressure spectra obtained by the Lighthill analogy and by PCWE are compared.

2 MATHEMATICAL MODEL

For the sake of simplicity a two-dimensional FSAI problem is considered. The FSI domain, schematically shown in Figure 1, is a subset of a substantially larger domain of sound propagation, see Figure 2. The FSI domain consists of the domain Ω^s_{ref}, representing the elastic structure (the vocal folds), and the domain Ω^f_{ref} occupied by fluid. The deformation of the elastic structure is described in the Lagrange coordinates. The domain Ω^f_{ref} denotes the reference fluid domain, e.g. the domain at the time instant $t = 0$ with

the common interface $\Gamma_{\mathrm{W_{ref}}} = \Gamma_{\mathrm{W_0}}$ between the fluid and the structure domain. The time evolution of the reference domain Ω^f_{ref} to the deformed domain Ω^f_t as well as the reference interface $\Gamma_{\mathrm{W_{ref}}}$ to the interface $\Gamma_{\mathrm{W_t}}$ at any time instant t is described by the ALE method.

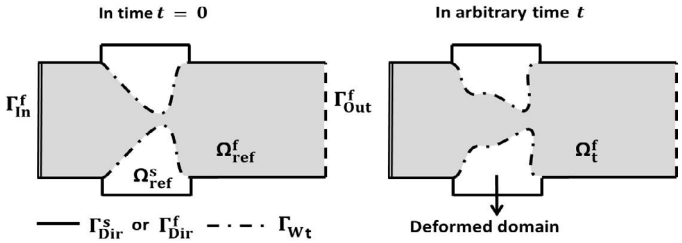

Figure 1: Schematic figure of vocal folds model and fluid domain with boundaries marked before (left) and after (right) a deformation.

2.1 Elastic body

The unknown deformation vector $\mathbf{u}(X,t) = (u_1, u_2)$ of the elastic body Ω^s is sought as a solution of the partial differential equation

$$\rho^s \frac{\partial^2 u_i}{\partial t^2} - \frac{\partial \tau^s_{ij}(\mathbf{u})}{\partial X_j} = f_i{}^s \quad \text{in } \Omega^s \times (0,\mathrm{T}). \tag{1}$$

This equation expresses the dynamic equilibrium between the inertia force and applied volume and surface forces. The structure density is denoted as ρ^s, the tensor τ^s_{ij} is the Cauchy stress tensor, the vector $\mathbf{f}^s = (f^s_1, f^s_2)$ is the volume density of an acting force and $X = (X_1, X_2)$ are the reference coordinates. Under the assumption of the linear relation between the displacement and the stress the generalized Hook law can be used, which for the isotropic case reads

$$\tau^s_{ij} = \lambda^s (\mathrm{div}\ \mathbf{u})\, \delta_{ij} + 2\mu^s e^s_{ij}, \tag{2}$$

where λ^s, μ^s are Lamé coefficients depending on the Young modulus of elasticity E^s and the Poisson ratio σ^s, see e.g. [12]. The tensor $\mathbb{I} = (\delta_{ij})$ is the Kronecker's delta and the tensor $\mathbf{e}^s = (e^s_{jk})$ is the strain tensor. For small displacements it has the form

$$e^s_{jk} = \frac{1}{2}\left(\frac{\partial u_j}{\partial X_k} + \frac{\partial u_k}{\partial X_j}\right). \tag{3}$$

Equation (1) is supplied by the initial and boundary conditions

$$\begin{aligned}
&\text{a)} && \mathbf{u}(X,0) = \mathbf{u}_0(X),\ \frac{\partial \mathbf{u}}{\partial t}(X,0) = \mathbf{u}_1(X) && \text{for } X \in\ \Omega^s,\\
&\text{b)} && \mathbf{u}(X,t) = \mathbf{u}_{\mathrm{Dir}}(X,t) && \text{for } X \in \Gamma^s_{\mathrm{Dir}},\ t \in (0,\mathrm{T}),\\
&\text{c)} && \tau^s_{ij}(X,t)\, n^s_j(X) = q^s_i(X,t), && \text{for } X \in \Gamma^s_{\mathrm{W_t}},\ t \in (0,\mathrm{T}),
\end{aligned} \tag{4}$$

where the $\Gamma_{\mathrm{W_{ref}}}, \Gamma^s_{\mathrm{Dir}}$ are mutually disjoint parts of the boundary $\partial\Omega^s = \Gamma_{\mathrm{W_{ref}}} \cup \Gamma^s_{\mathrm{Dir}}$ (see Figure 1) and $n^s_j(X)$ are components of the unit outer normal to $\Gamma_{\mathrm{W_{ref}}}$.

2.2 ALE method

One of the standard methods, which enable to solve the fluid flow in a time-dependent domain, is the ALE method. The basis of this method is the construction of a diffeomorphism A_t which maps the reference (undistorted) domain $\Omega^f_{\rm ref}$ on to the domain Ω^f_t at any instant time $t \in (0, \mathrm{T})$. The ALE domain velocity $\mathbf{w}_D$ under assumption of continuity of derivatives $\frac{\partial A_t}{\partial t} \in C(\overline{\Omega^f_{\rm ref}})$ is defined as

$$\mathbf{w}_D(A_t(X), t) = \frac{\partial}{\partial t} A_t(X), \quad t \in (0, \mathrm{T}),\ X \in \Omega^f_{\rm ref}. \tag{5}$$

The ALE derivative is then introduced as the time derivative with respect to a fixed point $X \in \Omega^f_{ref}$. It satisfies the following relation

$$\frac{D^A}{Dt} f(x,t) = \frac{\partial f}{\partial t}(x,t) + \mathbf{w}_D(x,t) \cdot \nabla f(x,t). \tag{6}$$

More details and practical construction of ALE mapping is described e.g. in [2] or [14].

2.3 Fluid flow

The motion of the viscous incompressible fluid in time-dependent domain Ω^f_t is described by the fluid velocity $\mathbf{v}(x,t)$ and the kinematic pressure p. This pair of unknowns obey the Navier-Stokes equations in the ALE form, see [2]

$$\frac{D^A \mathbf{v}}{Dt} + ((\mathbf{v} - \mathbf{w}_D) \cdot \nabla)\mathbf{v} - \nu^f \Delta \mathbf{v} + \nabla p = \mathbf{0}, \quad \text{div } \mathbf{v} = 0 \quad \text{in } \Omega^f_t, \tag{7}$$

where ν^f is the kinematic fluid viscosity.

The formulation of Navier-Stokes equations (fluid part of FSI problem) (7) is completed by zero initial and the following boundary conditions

$$\text{a)} \qquad \mathbf{v}(x,t) = \mathbf{w}_D(x,t) \qquad \text{for } x \in \Gamma^f_{\rm Dir} \cup \Gamma_{\rm W_t},\ t \in (0,\mathrm{T}), \tag{8}$$

$$\text{b)} \quad p(x,t)\mathbf{n}^f - \nu^f \frac{\partial \mathbf{v}}{\partial \mathbf{n}^f}(x,t) = -\frac{1}{2}\mathbf{v}(\mathbf{v}\cdot\mathbf{n}^f)^- + p_{\rm ref}\mathbf{n}^f \quad \text{for } x \in \Gamma^f_{\rm In} \cup \Gamma^f_{\rm Out},\ t \in (0,\mathrm{T}),$$

where $\mathbf{n}^f$ is unit outer normal to boundary $\partial\Omega^f_t$ and $p_{\rm ref}$ is a reference pressure (possibly different on the inlet $\Gamma^f_{\rm In}$ and the outlet $\Gamma^f_{\rm Out}$). The condition (8 b) is the modified do-nothing boundary condition, see e.g. [1].

2.4 Aeroacoustics

The acoustic domain Ω^a, where the acoustic problem is solved, is depicted in Figure 2. It is composed of three parts $\Omega^a_{\rm src}, \Omega^a_{\rm air}$ and $\Omega^a_{\rm pml}$, where $\overline{\Omega^a} = \overline{\Omega^a_{\rm src}} \cup \overline{\Omega^a_{\rm air}} \cup \overline{\Omega^a_{\rm pml}}$. The acoustic sources are calculated from the computed flow field in the domain $\Omega^a_{\rm src}$, which is

the same as reference fluid domain, i.e. $\Omega^a_{\text{src}} = \Omega^f_{\text{ref}}$. The change of domain Ω^a_{src} in time is neglected, the sources obtained on Ω^f_t are transformed back to the domain Ω^f_{ref} with the help of the ALE mapping. The domain Ω^a_{air} represents a part of the vocal tract behind the glottis up to mouth including a far field region, i.e. the outer space. The PML domain Ω^a_{pml} closes both the aforementioned domains in order to damp the outgoing sound waves.

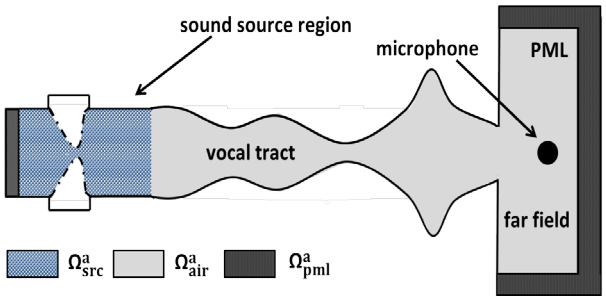

Figure 2: Scheme of acoustic domain. The propagation domain has tree parts – the sound source region, the vocal tract and the far field. Propagation region is enclosed by the PML region.

2.4.1 Lighthill analogy

The Lighthill analogy is inhomogenous wave equation

$$\frac{1}{c_0^2}\frac{\partial^2 p'}{\partial t^2} - \frac{\partial^2 p'}{\partial x_i^2} = \frac{\partial^2 T_{ij}}{\partial x_i \partial x_j}, \tag{9}$$

for unknown pressure fluctuation p' with known values of the Lighthill tensor T_{ij} and a given speed of sound c_0. This equation was derived by Lighthill in 1952 from compressible Navier-Stokes equations under supposition that acoustic waves with origin in a small source region propagate through a voluminous medium in rest state characterized by $\mathbf{v}_0 = \mathbf{0}, p_0$ and rest fluid density ρ^f_0. The formation of sound is here imaginary caused by acting force in the form of Lighthill tensor divergence, see [6]. The components of the Lighthill tensor T_{ij} are given by

$$T_{ij} = \rho^f v_i v_j + ((p - p_0) - c_0^2(\rho^f - \rho^f_0))\delta_{ij} - \tau^f_{ij}, \tag{10}$$

where τ^f_{ij} is the fluid viscous stress tensor. In next the Lighthill tensor is approximated by $T_{ij} \approx \rho^f v_i v_j$, where the viscous stress τ^f_{ij} and the stresses connected with the heat conduction $(p' - c^2\rho')\delta_{ij}$ are neglected, see [6].

2.4.2 Perturbed convective wave equation

Another suitable choice of acoustic analogy is the PCWE. It is based on splitting of physical quantities into mean and fluctuating parts. The fluctuating variables consists of

acoustic parts and non-acoustic components, i.e. incompressible parts

$$p = \overline{p} + p_{ic} + p_a, \qquad \mathbf{v} = \overline{\mathbf{v}} + \mathbf{v}_{ic} + \mathbf{v}_a. \tag{11}$$

With the presumption of incompressible homoentropic flow the splitting leads to the following partial differential equation for $\mathbf{v}^a$ and p^a

$$\frac{\partial p^a}{\partial t} + \overline{\mathbf{v}} \cdot \nabla p^a + \rho_0^f c_0^2 \nabla \cdot \mathbf{v}^a = -\frac{D p_{ic}}{D t}, \qquad \frac{\partial \mathbf{v}^a}{\partial t} + \nabla(\overline{\mathbf{v}} \cdot \mathbf{v}^a) + \frac{1}{\rho_0^f} \nabla p^a = \mathbf{0}, \tag{12}$$

where the substantial derivative $\frac{D}{Dt}$ equals $\frac{D}{Dt} = \frac{\partial}{\partial t} + \overline{\mathbf{v}} \cdot \nabla$. For derivation and discussion see [4]. These equations can be rewritten into one with the help of acoustic potential ψ^a related to the acoustic particle velocity $\mathbf{v}^a = -\nabla \psi^a$ (acoustic velocity field is irrotational)

$$\frac{1}{c_0^2} \frac{D^2 \psi^a}{D t^2} - \Delta \psi^a = -\frac{1}{\rho_0^f c_0^2} \frac{D p_{ic}}{D t}, \tag{13}$$

For further details see [4]. Moreover for low velocities we can disregard convection $\overline{\mathbf{v}} = 0$ and the PCWE formulation (13) simplifies further to

$$\frac{1}{c_0^2} \frac{\partial^2 \psi^a}{\partial t^2} - \Delta \psi^a = -\frac{1}{\rho_0^f c_0^2} \frac{\partial p_{ic}}{\partial t}. \tag{14}$$

Eq. (14) is very similar to Eq. (9), but with a quite big advantage of only first time derivative of right hand source term.

The wave equation (9) or (13), (14) is equipped with the zero initial condition and the boundary of acoustic domain $\partial\Omega^a$ with the outer normal $\mathbf{n}^a$ is considered as sound hard

$$\frac{\partial p'}{\partial \mathbf{n}^a}(x,t) = 0 \quad \text{or} \quad \frac{\partial \psi^a}{\partial \mathbf{n}^a}(x,t) = 0 \qquad \text{for } x \in \partial\Omega^a,\ t \in (0, \mathrm{T}). \tag{15}$$

2.4.3 PML

To tackle the open-boundary problem in bounded domains the PML technique was used. A few additional layers of elements were added along the normal direction of boundaries, which represents interface with open space. Inside these layers the sound waves are effectively damped to zero without any reflection at the interface between propagation region and PML. We further refer to [5].

2.5 Coupling conditions

The FSAI problem is coupled problem of three physical fields. The FSI coupling as well as acoustics-structure has the form of boundary conditions on the common interface, where on the contrary the fluid-acoustics coupling has volumetric character. Only the

forward coupling between FSI and acoustics is used, e.g. the forward acoustic coupling has the form of the flow field postprocessing.

The elastic deformation in FSI problem has prescribed Neumann boundary condition representing the impact of the aerodynamic forces on the elastic body

$$q_i^s(X,t) = -\sum_{j=1}^{2} \sigma_{ij}^f(x)\, n_j^f(x), \quad x = X + \mathbf{u}(X,t),\ X \in \Gamma_{\mathrm{W_{ref}}}, \tag{16}$$

where $\sigma_{ij}^f = \rho^f \left(-p\delta_{ij} + \nu^f(\frac{\partial v_i}{\partial x_j} + \frac{\partial v_j}{\partial x_i})\right)$, $i,j \in \{1,2\}$ are the components of the fluid stress tensor.

The fluid flow problem is completed with the Dirichlet boundary condition postulated by equation (8 a), which represents the continuity between the fluid and the structure velocity across the boundary $\Gamma_{\mathrm{W_t}}$.

Moreover also the location of the interface $\Gamma_{\mathrm{W_t}}$ at time t is also variable and it depends on the solution of FSI problem. Its location corresponding to the force equilibrium between aerodynamic and elastic forces at time instant t and it is implicitly given by structure deformation $\mathbf{u}(t)$ as $\Gamma_{\mathrm{W_t}} = \{x \in \mathbb{R}^2 |\, x = X + \mathbf{u}(X,t),\ X \in \Gamma_{\mathrm{W_{ref}}}\}$.

3 NUMERICAL MODEL

All three subproblems given by partial differential equations (1), (7) and (9) or (14) are solved by the FEM based on the weak formulation in space. Obtained semi-discrete system is subsequently discretized in time by the finite difference scheme with the same constant time step $\Delta t = \frac{T}{N}, N >> 1$.

3.1 Acoustics

Equations (9) are reformulated in the weak sense with the aid of a test function η from the Sobolev space $W^{1,2}(\Omega^a)$, see [4]. The application of the Green theorem together with the definition of boundary condition (15) gives us the final form

$$\int_{\Omega^a} \frac{1}{c_0^2} \frac{\partial^2 p'}{\partial t^2} \eta \,\mathrm{d}x + \int_{\Omega^a} \nabla p' \cdot \nabla \eta \,\mathrm{d}x = -\int_{\Omega^a} (\mathrm{div}\,\mathbf{T}) \cdot \nabla \eta \,\mathrm{d}x. \tag{17}$$

Using the restriction of test functions to a finite element space and seeking the solution as a linear combination of the basis functions η_j with unknown time dependent coefficients $\boldsymbol{\gamma} = \boldsymbol{\gamma}(t)$ leads to

$$\mathbb{M}^a \ddot{\boldsymbol{\gamma}} + \mathbb{K}^a \boldsymbol{\gamma} = \mathbf{b}^a(t), \tag{18}$$

where the components of the vector $\mathbf{b}^a(t) = (b_i^a)$ and of the matrices $\mathbb{M}^a = (m_{ij}^a)$, $\mathbb{K}^a = (k_{ij}^a)$ are given as

$$b_i^a = -\int_{\Omega^a} (\nabla \cdot \mathbf{T}) \cdot \nabla \eta_i \,\mathrm{d}x, \quad m_{ij}^a = \int_{\Omega^a} \frac{1}{c_0^2} \eta_j \eta_i \,\mathrm{d}x, \quad k_{ij}^a = \int_{\Omega^a} \nabla \eta_j \cdot \nabla \eta_i \,\mathrm{d}x. \tag{19}$$

The derivation of the weak formulation of Eq. (13) or (14) is similar. System (18) is numerically discretized in time by the Newmark method.

3.2 Elastic body

The standard finite element discretization of problem (1) leads to the matrix system for the unknown time-dependent vector of coefficients $\boldsymbol{\alpha}(t)$, see e.g. [14], i.e.

$$\mathbb{M}\ddot{\boldsymbol{\alpha}} + \mathbb{C}\dot{\boldsymbol{\alpha}} + \mathbb{K}\boldsymbol{\alpha} = \mathbf{b}(t), \tag{20}$$

where matrices $\mathbb{M} = (m_{ij}), \mathbb{K} = (k_{ij})$ has elements

$$m_{ij} = \int_{\Omega^s} \rho^s \boldsymbol{\phi}_i \cdot \boldsymbol{\phi}_j \, \mathrm{d}X, \qquad k_{ij} = \int_{\Omega^s} \left(\lambda^s (\mathrm{div}\ \boldsymbol{\phi}_i)\, \delta_{rl} + 2\mu^s e^s_{rl}(\boldsymbol{\phi}_i)\right) e^s_{rl}(\boldsymbol{\phi}_j) \, \mathrm{d}X, \tag{21}$$

and the vector $\mathbf{b}(t)$ has components $b_i(t) = \int_{\Omega^s} \mathbf{f}^s \cdot \boldsymbol{\phi}_i \, \mathrm{d}X + \int_{\Gamma^s_{\mathrm{Neu}}} \mathbf{q}^s \cdot \boldsymbol{\phi}_i \, \mathrm{d}S$. The matrix $\mathbb{C} = \epsilon_1 \mathbb{M} + \epsilon_2 \mathbb{K}$ was added as the proportional damping with suitable parameters ϵ_1, ϵ_2. System (21) is numerically discretized in time by the Newmark method, see e.g. [2].

3.3 Fluid flow

The equation (7) is firstly discretized at arbitrary time step $t = t_{n+1}$ in time. The ALE derivative is approximated by the backward difference formula of second order

$$\frac{D^A \mathbf{v}}{Dt}(x, t_{n+1}) \approx \frac{3\mathbf{v}^{n+1}(x_{n+1}) - 4\mathbf{v}^n(x_n) + \mathbf{v}^{n-1}(x_{n-1})}{2\Delta t}, \quad x_i = A_{t_i}(A^{-1}_{t_{n+1}}(x)). \tag{22}$$

For the sake of simplicity in the next section the time index $^{n+1}$ will be omitted. By multiplication of equations (7) by a test function $\boldsymbol{\varphi} \in \mathbf{W}^{1,2}(\Omega^f)$ and $q \in L^2(\Omega^f)$, integration over Ω^f and by using Green theorem the standard weak spatial formulation is obtained, see e.g. [2]. One extra application of Green theorem used partially for the convective term delivers the formulation based on the analysis in [1] or described in [14]. The substitution of test spaces with finite element spaces $\mathbf{X}_h \subset \mathbf{W}^{1,2}(\Omega^f), M_h \subset L^2(\Omega^f)$ let us to write the approximative solution $\mathbf{v}_h, p_h$ as linear combinations

$$\mathbf{v}_h(x,t) = \sum_{j=1}^{2N_h^v} \beta_j^v(t)\, \boldsymbol{\varphi}_j(x), \qquad p_h(x,t) = \sum_{j=1}^{N_h^p} \beta_j^p(t)\, q_j(x), \tag{23}$$

where $\boldsymbol{\varphi}_j, q_j$ are finite element base functions of the spaces $\mathbf{X}_h, M_h$. This approach yields the matrix system

$$\begin{pmatrix} \mathbb{A}(\mathbf{v}_h) & \mathbb{B} \\ \mathbb{B}^T & 0 \end{pmatrix} \begin{pmatrix} \boldsymbol{\beta}^v \\ \boldsymbol{\beta}^p \end{pmatrix} = \begin{pmatrix} \mathbf{g} \\ \mathbf{0} \end{pmatrix}, \tag{24}$$

where $\mathbb{A}(\mathbf{v}_h) = \frac{1}{\Delta t}\mathbb{M} + \mathbb{C}(\mathbf{v}_h) + \mathbb{D}$. The elements of the matrices $\mathbb{M} = (m_{ij}), \mathbb{C} = (c_{ij})$, $\mathbb{D} = (d_{ij}), \mathbb{B} = (b_{ij})$ and the vector components $\mathbf{g} = (g_i)$ are given by

$$m_{ij} = \frac{3}{2}\int_{\Omega^f} \boldsymbol{\varphi}_j \cdot \boldsymbol{\varphi}_i \,\mathrm{d}x, \quad d_{ij} = \int_{\Omega^f} \nu^f \,\nabla\boldsymbol{\varphi}_j \cdot \nabla\boldsymbol{\varphi}_i \,\mathrm{d}x, \quad b_{ij} = \int_{\Omega^f} -q_j \,\mathrm{div}\, \boldsymbol{\varphi}_i \,\mathrm{d}x, \quad (25)$$

$$2 \cdot c_{ij} = \int_{\Omega^f} ((\mathbf{v}_h - 2\mathbf{w}_D^{n+1}) \cdot \nabla)\boldsymbol{\varphi}_j \cdot \boldsymbol{\varphi}_i - (\mathbf{v}_h \cdot \nabla)\boldsymbol{\varphi}_i \cdot \boldsymbol{\varphi}_j \,\mathrm{d}x + \int_{\Gamma^f_{\mathrm{Out}} \cup \Gamma^f_{\mathrm{In}}} (\mathbf{v}_h \cdot \mathbf{n}^f)^+ \boldsymbol{\varphi}_j \cdot \boldsymbol{\varphi}_i \,\mathrm{d}S,$$

$$g_i = \int_{\Omega^f} \frac{4\overline{\mathbf{v}}^n - \overline{\mathbf{v}}^{n-1}}{2\Delta t} \cdot \boldsymbol{\varphi}_i \,\mathrm{d}x - \int_{\Gamma^f_{\mathrm{Out}} \cup \Gamma^f_{\mathrm{In}}} p_{ref}\, \boldsymbol{\varphi}_i \cdot \mathbf{n}^f \,\mathrm{d}S.$$

The system of equations (24) is non-linear. For its solution the linearization $\mathbf{v}_h = \mathbf{v}^n$ is used together with the linear algebra solver from the library UMFPACK. The fluid FEM solver is stabilized by the streamline-upwind/Petrov-Galerkin, the pressure-stabilization/Petrov-Galerkin and 'div-div' stabilization method. It keeps the method stable, consistent and still accurate, see e.g. [3] or for the implementation details [2].

3.4 Algorithm

The advantage of chosen hybrid approach is that sound sources acting on right hand side of acoustic analogies can be computed anytime later from the solution of FSI problem. The partitioned FSI scheme was implemented with the strong coupling, for details see [2].

4 Numerical results

During the whole computation the time step was kept constant $\Delta t = 2.5 \cdot 10^{-5}\,\mathrm{s}$.

4.1 FSI problem

The vocal fold (VF) model shape consisting of four layers and their material parameters were adopted from the article [15] together with initial gap between VFs 2.0 mm. The damping parameters were chosen as $\epsilon_1 = 5\,\mathrm{s}^{-1}, \epsilon_2 = 2.0 \cdot 10^{-5}\,\mathrm{s}$ and the densities $\rho^s = 1000\,\mathrm{kg/m^3}$, $\rho^f = 1.185\,\mathrm{kg/m^3}$ and kinematic viscosity $\nu^f = 1.47 \cdot 10^{-5}\,\mathrm{m/s^2}$ was set.

The FSI problem was solved with the prescribed pressure difference between inlet and outlet with value $p_{\mathrm{ref}} = 2000\,\mathrm{Pa} \cdot \mathrm{m^3/kg}$. The full FSI interaction was enabled at 0.01 s and after a short transition behaviour the typical evolution of the flow induced vibration of VF appeared, see Figure 3. The excitation of first two eigenmodes of VF can be identified with the help of the Fourier transform. These results are in good correspondence with results of paper [15].

4.2 Aeroacoustics

The shape of vocal tract model for vowel \u\ are taken from MRI measurement – [13], where the length is modified due to the smooth connection between the end of the fluid computational domain and the start of sharply narrowing vocal tract domain.

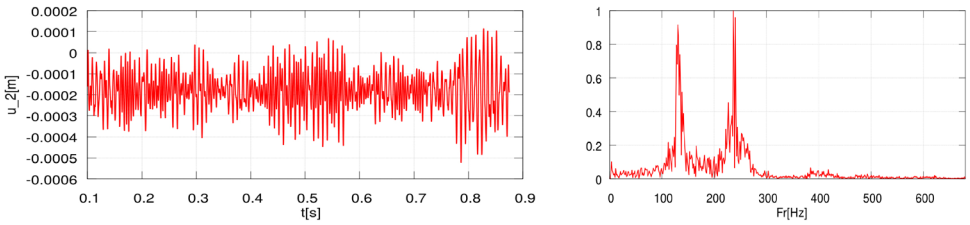

Figure 3: On the left - time behaviour of y-displacement of chosen point from the top of bottom VF. The displacement stored from $t = 0.1\,\mathrm{s}$. On the right - (normalized) Fourier transform of time signal from the left.

Since the acoustic problem does not require so fine grid, the sound source terms of Eq. (9) and (14) were interpolated onto coarser acoustic mesh during their calculation. The computed sound sources were further investigated by Fourier transform. The Figure 4 shows a comparison of the contributions with frequencies 235 and 1371 Hz obtained by different analogies. The sound source density with frequency 235 Hz corresponds to the VF excitation frequency and it is mainly located inside the glottis. The second density with nonharmonic frequency 1371 Hz is distributed in turbulent region behind glottis. It is associated with vorticity of the glottal jet and it has smaller magnitude. Similar character of results was obtained in [11]. The sources of Lighthill analogy is quite sensitive to the high velocity gradients due to the need of second space derivatives, which can lead to numerical artifacts.

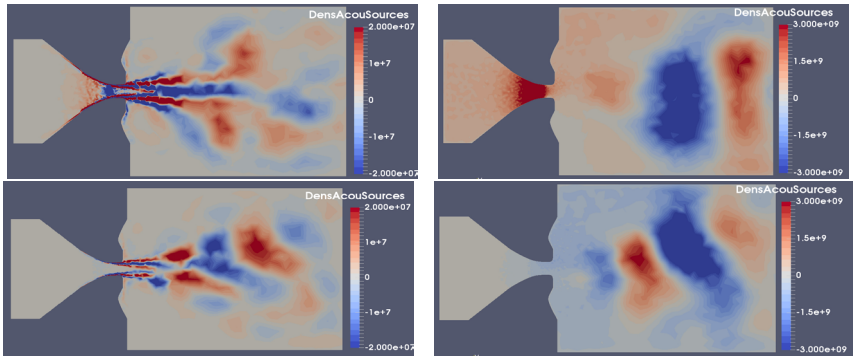

Figure 4: The computed sound source densities for Lighthill analogy on the left and for PCWE on the right for frequencies of 235 (up) and 1371 Hz (down).

Finally, the acoustic simulation was performed in the whole domain Ω^a. The acoustic pressure was monitored outside the mouth at the microphone position ($x = 0.24\,\mathrm{m}, y = 0\,\mathrm{m}$). The Fourier transform of acoustic pressure is depicted in Figure 5. The obtained frequencies for the PCWE case do not coincide with the frequencies of first formants of measured natural pronunciation of vowel \u\ in [13] (black lines in Figure 5). But the frequency peaks quite well answer the peaks of transfer function for vocal tract domain Ω^a_{air} at least for frequencies higher than 1500 Hz, see Figure 5. The differencies can be

caused by the aforementioned prolongation. The frequencies acquired for the Lighthill case do not demostrate agreetment with PCWE results. The effect of vocal tract filtering is clearly visible for higher frequencies.

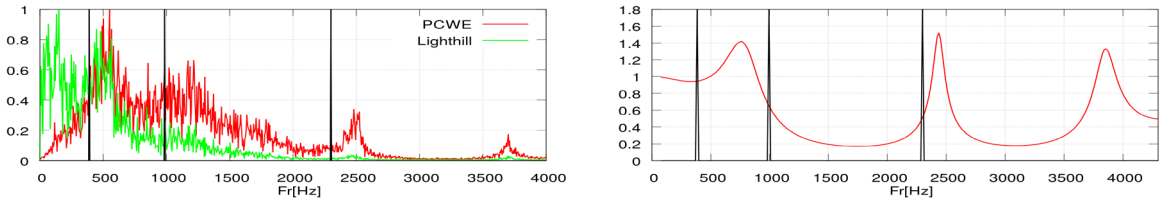

Figure 5: On the left - normalised Fourier transform of acoustic pressure measured at microphone position computed from 0.9 s signal length. The black vertical lines mark the frequencies 389 Hz, 987 Hz and 2299 Hz taken from article [13]. On the right - transfer function of chosen shape of vocal tract.

5 CONCLUSIONS

In this contribution the mathematical description of the FSAI is presented, where the hybrid partitioned approach was applied. The Lighthill acoustic analogy and PCWE approach were utilized for the calculation of the acoustic sources and simulation of their propagation through vocal tract model. The all three physical problems are numerically solved by the FEM. The fluid solver was stabilized by SUPG, PSPG and 'div-div' method. The results of flow induced vibration of vocal folds were computed and postprocessed by in-house developed program to determine the sound sources. They were analysed in frequency domain and then their propagation through vocal tract was simulated by CFS++ solver. The obtained results by PCWE and by Lighthill analogy do not show high correspondence.

Acknowledgment

Authors are grateful for possibility to use *C*FS++ scientific FE library. The financial support for this project was provided by the *Grant No. SGS16/206/OHK2/3T/12* of CTU in Prague.

REFERENCES

[1] M. Braack and P. B. Mucha. Directional do-nothing condition for the Navier-Stokes equations. *Journal of Computational Mathematics*, 32:507–521, 2014.

[2] M. Feistauer, P. Sváček, and J. Horáček. Numerical simulation of fluid-structure interaction problems with applications to flow in vocal folds. In T. Bodnár, G. P. Galdi, and S. Nečasová, editors, *Fluid-structure Interaction and Biomedical Applications*, pages 312–393. Birkhauser, 2014.

[3] Tobias Gelhard, Gert Lube, Maxim A. Olshanskii, and Jan-Hendrik Starcke. Stabilized finite element schemes with LBB-stable elements for incompressible flows. *Journal of Computational and Applied Mathematics*, 177(2):243–267, 2005.

[4] Andreas Hüppe and Manfred Kaltenbacher. Spectral finite elements for computational aeroacoustics using acoustic perturbation equations. *Journal of Computational Acoustics*, 20(02):1240005, 2012.

[5] Barbara Kaltenbacher, Manfred Kaltenbacher, and Imbo Sim. A modified and stable version of a perfectly matched layer technique for the 3-d second order wave equation in time domain with an application to aeroacoustics. *Journal of computational physics*, 235:407–422, 2013.

[6] Michael J Lighthill. On sound generated aerodynamically. i. general theory. In *Proceedings of the Royal Society of London A: Mathematical, Physical and Engineering Sciences*, volume 211, pages 564–587. The Royal Society, 1952.

[7] R. Mittal, B. D. Erath, and M. W. Plesniak. Fluid dynamics of human phonation and speech. *Annual Review of Fluid Mechanics*, 45:437–467, 2013.

[8] Petra Pořízková, Karel Kozel, and Jaromír Horáček. Numerical solution of compressible and incompressible unsteady flows in channel inspired by vocal tract. *Journal of Computational and Applied Mathematics*, 270:323–329, 2014.

[9] Robert J Ruben. Redefining the survival of the fittest: communication disorders in the 21st century. *The Laryngoscope*, 110(2):241–241, 2000.

[10] Rüdiger Schwarze, Willy Mattheus, Jens Klostermann, and Christoph Brücker. Starting jet flows in a three-dimensional channel with larynx-shaped constriction. *Computers & Fluids*, 48(1):68–83, 2011.

[11] P. Šidlof, S. Zörner, and A. Hüppe. A hybrid approach to the computational aeroacoustics of human voice production. *Biomechanics and Modeling in Mechanobiology*, 14(3):473–488, oct 2014.

[12] William S. Slaughter. *Linearized Elasticity Problems*. Springer, 2002.

[13] Brad H Story, Ingo R Titze, and Eric A Hoffman. Vocal tract area functions from magnetic resonance imaging. *The Journal of the Acoustical Society of America*, 100(1):537–554, 1996.

[14] J. Valášek, P. Sváček, and J. Horáček. Numerical solution of fluid-structure interaction represented by human vocal folds in airflow. In Vesely M. and Dancova P., editors, *EFM15 Experimental Fluid Mechanics 2015*, volume 114. EPJ Web of Conferences, March 2016.

[15] S. Zörner, M. Kaltenbacher, and M. Döllinger. Investigation of prescribed movement in fluid-structure interaction simulation for the human phonation process. *Computers & Fluids*, 86:133–140, 2013.